

Stellar Migration by Short Lived Density Peaks Arising from Interference of Spiral Density Waves in an N-body Simulation

Justin Comparetta, & Alice C. Quillen

Department of Physics and Astronomy, University of Rochester, Rochester, NY 14627, USA;

30 October 2018

ABSTRACT

We identify migrating stars in an N-body hybrid simulation of a Milky-Way-like disk. Outward migration can occur when a star in a low eccentricity orbit lags a short-lived local spiral arm density peak. We interpret short lived local density peaks, that appear and fade on approximately an orbital period, as arising from positive interference between spiral density wave patterns that are longer lived. We find that stars near such a peak can migrate over a significant distance in galactocentric radius during the peak lifetime, providing that the peak is sufficiently dense. We propose that short lived density peaks, caused by interference between spiral density waves, can induce radial migration even when there are no spiral density waves that are strong near their corotation resonance. Using a Gaussian bar model for the potential perturbation associated with a narrow transient spiral feature, estimates of the migration rate, angular offset between particle and spiral feature, and maximum eccentricity for migrators roughly agrees with the values measured in our simulation. When multiple spiral density waves are present, local density peaks can appear and disappear on timescales faster than the timescale estimated for growth and decay of individual waves and the peak surface density can be larger than for any individual wave. Consequently, migration induced by transient density peaks may be more pervasive than that mediated by the growth and decay of individual patterns and occurring at their corotation resonance. We discuss interpretation of transient-like behavior in terms of interfering patterns, including estimating a coherence time for features that appear due to constructive interference, their effective angular rotation rates and the speed and direction that a density maximum would move across a galaxy inducing a localized and traveling burst of star formation.

1 INTRODUCTION

Bar and spiral structures can change the mean orbital radius or guiding centers of stars and so migrate them from their birth radius (Wielen 1977; Fuchs & Wielen 1987; Wielen et al. 1996; Sellwood & Binney 2002; Roskar et al. 2008; Minchev et al. 2011; Roskar et al. 2012; Grand et al. 2012a,b). The resulting radial mixing is required to account for stellar metallicity distributions (Schönrich & Binney 2009). Many stars, including the Sun, (Adams 2010), were born in a cluster, (Eggen 1992; De Silva et al. 2007; Bubar & King 2010) that then dissolved or dispersed to other radii in the Galaxy (Wielen 1977; Wielen et al. 1996; Portegies Zwart 2009; Brown et al. 2010; Bland-Hawthorn et al. 2010). Understanding migration and heating mechanisms in the stellar disk is needed to interpret forthcoming surveys of stars in the Galaxy.

Transient spiral structure (Sellwood & Carlbert 1984; Toomre 1990; Toomre & Kalnajs 1991; Baba et al. 2009; Fujii et al. 2011; Sellwood 2011), causing both heating and

migration, has been modeled as a diffusive stochastic process (Jenkins & Binney 1990; Schönrich & Binney 2009; Bland-Hawthorn et al. 2010). One difficulty of this approach arises from the small number of Galactic rotation periods in a Hubble time. The rotation period of the Sun is about 250 Myr, giving only 40 rotation periods during the lifetime of the Galactic disk. If spiral arms require a few rotation periods to grow and decay, then only about a dozen non-interfering patterns can arise during the lifetime of the Galactic disk. Recent studies suggest that multiple patterns can co-exist in a galactic disk (Henry et al. 2003; Naoz & Shaviv 2007; Meidt et al. 2009; Quillen et al. 2011; Sellwood 2011). Only if multiple patterns grow and decay in an uncorrelated or non-interfering way can stochastic models for radial migration be adapted in a straightforward manner to model radial migration. Interference between patterns may increase the heating rate (Minchev & Quillen 2006; Minchev et al. 2012), induce chaos in the dynamics (Quillen 2003), account for star formation in armlets (Henry et al. 2003), gaps in local velocity distributions (Quillen et al. 2011), and modify disk

surface brightness profiles (Minchev et al. 2012). We focus here on how the presence of multiple spiral density waves influences stellar migration.

Stellar migration can occur when a star is temporarily trapped in the corotation region (or resonance) of a spiral density wave (Lynden Bell & Kalnajs 1972; Sellwood & Binney 2002). We outline the physical mechanism as proposed and described by Sellwood & Binney (2002). The star is captured into the corotation resonance as the spiral density wave grows. When there is a fixed rotating spiral perturbation, the Jacobi integral, $E_J = E - L\Omega_s$, is conserved. Here E and L are the energy and z component of the star’s angular momentum per unit mass, and Ω_s is the pattern speed of the spiral density wave. The star can vary in angular momentum, L , while the spiral density wave is strong. After the spiral density wave dissipates, the star can be left at a different angular momentum, but may not have significantly increased in eccentricity. A number of numerical studies have supported this migration mechanism, including the seminal work Sellwood & Binney (2002), but also Roskar et al. (2008) using SPH simulations, and recently Grand et al. (2012a,b) in both N-body and SPH/N-body simulations. Grand et al. (2012a,b) illustrated that outward migrating stars lagged a spiral density peak and vice-versa for inwards migrating stars. They also showed that migrating stars remained on nearly circular orbits, as would be expected when E_J is conserved and $\Omega \approx \Omega_s$ during migration. Here Ω is the angular rotation rate of the migrating star. Distributions of the change in angular momentum as a function of initial angular momentum, ΔL vs L_0 , from numerical simulations (Sellwood & Binney 2002; Roskar et al. 2012; Minchev et al. 2012), exhibit features at corotation resonances, with positive variations in ΔL occurring inside corotation and vice-versa outside of the resonance. The theory (as outlined by Sellwood & Binney 2002) for migration due to a corotation resonance is simplest in the presence of a single slowly growing and then fading spiral pattern. We examine here how this mechanism might be modified in the presence of multiple spiral density waves.

In this paper we examine migration in a simulation with multiple spiral density waves. We study individual migrating particles to probe the mechanism accounting for their rapid variations in angular momentum. We then discuss modifications to the corotation mechanism for radial migration in a setting with multiple spiral density waves.

2 MIGRATION IN AN N-BODY SIMULATION

We use the disk galaxy simulation previously described and studied by Quillen et al. (2011). The initial conditions for the simulations were for a model Milky Way galaxy, generated with numerical phase distribution functions using the method discussed by Widrow et al. (2008). Spectrograms were used to identify a bar and three spiral patterns in this simulation, two with two arms, ($m = 2$), and one with three arms ($m = 3$, see Table 1 by Quillen et al. 2011). The spiral structure (shown in $\log r$ vs angle) shown in Figure 3 by Quillen et al. (2011) can be compared with similar figures of other studies (see Figure 9 by Grand et al. 2012a and 10 by Grand et al. 2012b). While $m = 2$ and 3 structures dominate our simulation and that by Grand et al. (2012b),

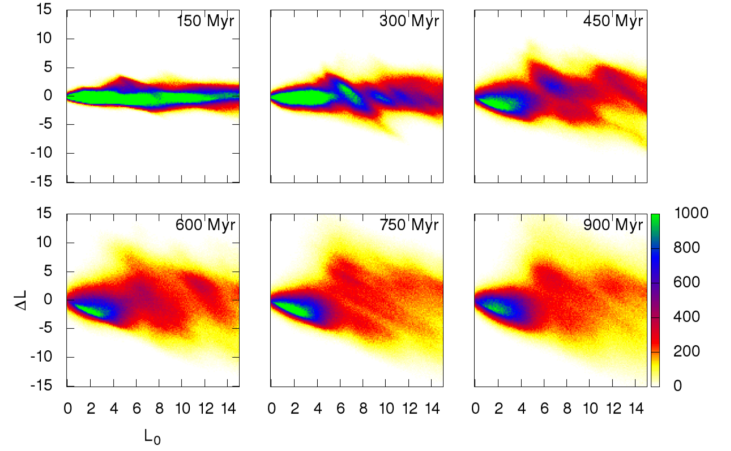


Figure 1. Histograms of the numbers of stars that experienced a change in angular momentum, ΔL (shown on the y -axis), versus initial angular momentum, L_0 (x -axis), for the disk particles in the simulation. From left to right the histograms are shown every 0.3 Gyr. Here L_0 and ΔL are in units of $100 \text{ km s}^{-1} \text{ kpc}$.

the one studied by Grand et al. (2012a) is dominated by patterns with higher numbers of arms (m between 3–7) and has a flocculent rather than grand-design morphology.

In Figure 1 we show a histogram of changes in angular momentum, ΔL , computed every 0.15 Gyr, as a function of initial angular momentum, L_0 , in units of $100 \text{ km s}^{-1} \text{ kpc}$ for the disk particles in the simulation. As have previous studies (e.g., Roskar et al. 2012; Minchev et al. 2012), we see a strong feature associated with the bar’s corotation radius at $L_0 \sim 8 \text{ km s}^{-1} \text{ kpc}$, moving progressively outwards as the bar slows down. However, changes in angular momentum occur all over the galaxy and changes in angular momentum persist after the bar has grown. This migration cannot be mediated by the growth and decay of the bar’s corotation resonance as the bar does not decay. We conclude that migration is pervasive and on-going. Because of the number of spiral density waves, this is perhaps not surprising. However, the spectrograms (see Figures 4–6 by Quillen et al. 2011) show that the stronger patterns in the simulation contain little power at their corotation radii. Only the bar and the $m = 3$ pattern contain power near corotation (see Figure 6 by Quillen et al. 2011). A similar problem was discussed by Grand et al. (2012a) whose spectrograms showed that most spectral features were strong at frequencies above or below corotation (see their Figure 6). Nevertheless they also found that radial migration occurred in their simulation. Grand et al. (2012b) illustrated extreme migration near the end of their bar, and we see from the ΔL vs L_0 histograms that migration in our simulation occurs in the same region.

2.1 Finding migrators

We identify particles that migrate large distances in the following manner. We first identified particles with an overall change in angular momentum of $15 < |\Delta L| < 50 \text{ km s}^{-1} \text{ kpc}$. Of these ‘extreme migrators’, a randomly selected sample were inspected for radial movement in proximity to the bar and spiral arms. Of these we chose a single fiducial particle to study in more detail. In Figure 2a we

show the trajectory of a particle that migrated from radius $r = 4.1$ kpc at 500 Myr to 8.6 kpc at 750 Myr, along with 39 other particles that were near, (within 0.1 kpc in galactocentric radius and 5° in azimuthal angle) the chosen particle at 500 Myrs, the start of the chosen particle's outward migration. The positions of these particles are shown at 525 Myr (just after they are all in the same region) and at 25 Myr intervals afterwards. At 500 Myr, all 40 of these particles have similar angular momentum (within 25 km s^{-1} kpc of the chosen particle), however they do not all have the same radial velocity. We use u to denote the radial velocity component in galactocentric coordinates with convention positive u for a particle moving toward the galactic center. In Figure 2a particles with $u \leq -30 \text{ km s}^{-1}$ are shown as asterisks and include the chosen particle, the filled squares are those with $u \geq 30$, and the open squares with $|u| < 30 \text{ km s}^{-1}$. Even though the chosen particle is in a nearly circular orbit (and has little epicyclic motion) it has a negative u corresponding to an outward drift.

The positions of the 40 particles are shown in Figure 2a along with the disk density in cylindrical galactocentric coordinates. The azimuthally averaged value of the surface density has been subtracted at each radius. The x -axis is the azimuthal angle, θ , in degrees and the y -axis is \log_{10} radius in kpc. Rotation is in the positive θ direction (moving to the right in Figure 2a) and the spiral structures are trailing with a pitch angle of approximately 24° (as measured previously by Quillen et al. 2011). During the time 500 to 750 Myr the chosen particle, and many of the particles with similar initial velocities, lag just behind a strong local density feature and it is during this time that the particle moves outwards. The local density peak exerts a force in the azimuthal direction on the particle. This force gives a torque that causes the particle's angular momentum to increase. As long as the particle remains approximately the same distance away from the density peak and lags the peak, it continues to gain angular momentum and moves outwards.

Our fiducial or chosen particle is used in a number of Figures. Shown in Figure 3 is the surface density as a function of angle, at three different times during the migration for our selected particle. The angular difference between this particle and nearest density peak is shown in Figure 4. The density of the nearest peak and radial migration rate for the same particle are plotted in Figure 5.

At every timestep we measured the angular distance between our fiducial particle (one of the asterisks in Figure 2a) and the nearest density peak. We denote the angle difference, $\Delta\theta \equiv \theta_{peak} - \theta_p$, between the azimuthal angle of the nearest spiral density peak, θ_{peak} , and the particle, θ_p ; We measure θ_{peak} by computing the surface density as a function of azimuthal angle in an annulus with mean radius equivalent to that of the particle and with radial width 0.2 kpc. Within this annulus we located the highest local maximum disk surface density that was less than 45° away from the particle, and recorded the angle of this peak. Shown in Figure 3 is the surface density as a function of $\theta - \theta_p$, at three different times during the migration for our selected particle. At each time there is a nearby (within 45°) density peak. The particle lags the nearest density peak and this is consistent with its outwards migration. Figure 3 also shows the surface density in units of $M_\odot \text{ pc}^{-2}$. In subsequent discussion we will use the surface density of the nearest peak to estimate

the migration rate of the particle. The estimated migration rate will then be compared to the actual migration rate.

Plotted in Figure 4a is the rate of change of angular momentum, \dot{L} , in units of $\text{kpc}^2 \text{ Myr}^{-2}$, as a function of time, for the selected particle along with the the difference between the azimuthal angle of the nearest spiral density peak and the particle, $\Delta\theta$. On the bottom panel of the plot we also show the particle's radius as a function of time. The angular rotation in this simulation has positive $d\theta/dt$ corresponding to counter-clockwise rotation. Consequently our plotted angle, $\Delta\theta$, is positive when the particle lags the peak. We see from Figure 4a that the particle moves outwards (\dot{L} is positive and radius increases) when the particle lags the nearest density peak ($\Delta\theta > 0$).

Our illustration that a particle migrates outward when it lags a density peak is similar and consistent with the similar illustrations by Grand et al. (2012a,b). The corotation resonance model for migration (Sellwood & Binney 2002) predicts that the particle would be out of phase with a potential perturbation while it drifts outwards. In this manner, the offset between particle and density peak seen in our simulation is consistent with the corotation resonance model for migration.

Figure 4a also shows the particle radius as a function of time. When the particle's eccentricity is non-zero the particle oscillates radially (known as the epicycle). Previous studies have found that corotation resonances are only effective at causing migration among low eccentricity particles (see Figure 12 by Minchev et al. 2012 and associated discussion). We can see in Figure 4 that the particle only migrates when the particle eccentricity is low and that the eccentricity does not increase during migration. The positive radial velocity value for migrating particles was due to their outward drift rather than epicyclic oscillations. The corotation resonance model for migration by Sellwood & Binney (2002) is consistent with the lack of eccentricity variation during migration. Figure 2a shows that particles that have radial velocity u differing by $30\text{--}40 \text{ km s}^{-1}$ from our extreme migrators fail to migrate. For particles nearly in circular orbits, eccentricity can be estimated from a maximum u value as $e \sim u/v_c$. Hence we crudely estimate that only particles with eccentricity $e \lesssim 0.2$ migrate in the vicinity of our fiducial particle and a maximum migrator eccentricity of $e_{max} \sim 0.2$.

Figure 4b we show a particle from Figure 2a which does not migrate significantly. As also seen in the case in which the particle migrated, this particle has positive \dot{L} when lagging the nearest density peak, but also negative \dot{L} when leading the nearest density peak. As these periods of lagging and leading occur for similar durations and distances to the peak location, this particle does not migrate outward like the particle shown in Figure 4a.

2.2 The lifetime of a local density peak that can cause a star to migrate

The density feature or peak responsible for the migration of the star shown in Figure 2a appeared at a time of about 475 Myr and disappeared at a time of about 750 Myr and so lasted about 275 Myr. In this simulation the circular velocity is about 200 km s^{-1} and so the rotation period at a Galactocentric radius of 10 kpc is about 300 Myr. The local peak (causing migration of the particle with trajectory shown in

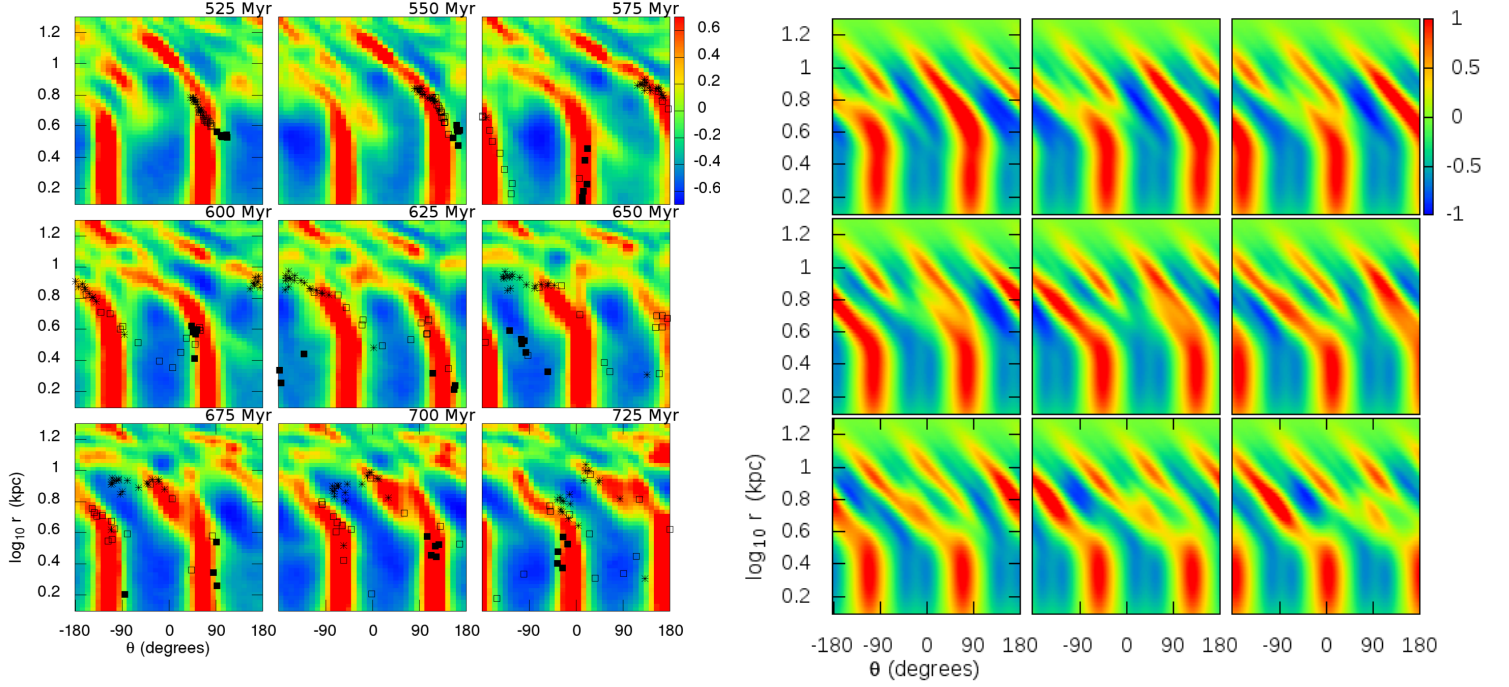


Figure 2. a) Position of 40 stars at different times. These 40 particles were all within 0.1 kpc of each other at 500 Myr, just before the top left panel. Each panel shows a different snapshot with snapshots plotted every 25 Myr, starting at 525 Myr. The stars are plotted on top of the surface density distribution in cylindrical coordinates. The x -axis gives azimuthal angle and the y -axis \log_{10} of the radius in kpc. In the plot, the stars marked with an asterisk have a radial velocity, $u \leq -30$, the filled squares $u \geq 30$, and the open squares $|u| < 30 \text{ km s}^{-1}$. The local density peak inducing migration lasted less than 300 Myr. Rotation is with positive $d\theta/dt$ so patterns move to the right. Low eccentricity stars migrate outwards when they lag (and follow) a local density peak in the disk. Only particles with small positive radial velocities move outwards. Particles with higher epicycles (the filled and many of the open squares) fail to migrate. b) Surface density distribution similar for the same times as a) but for the model described in section 2.4 with the parameters listed in Table 1.

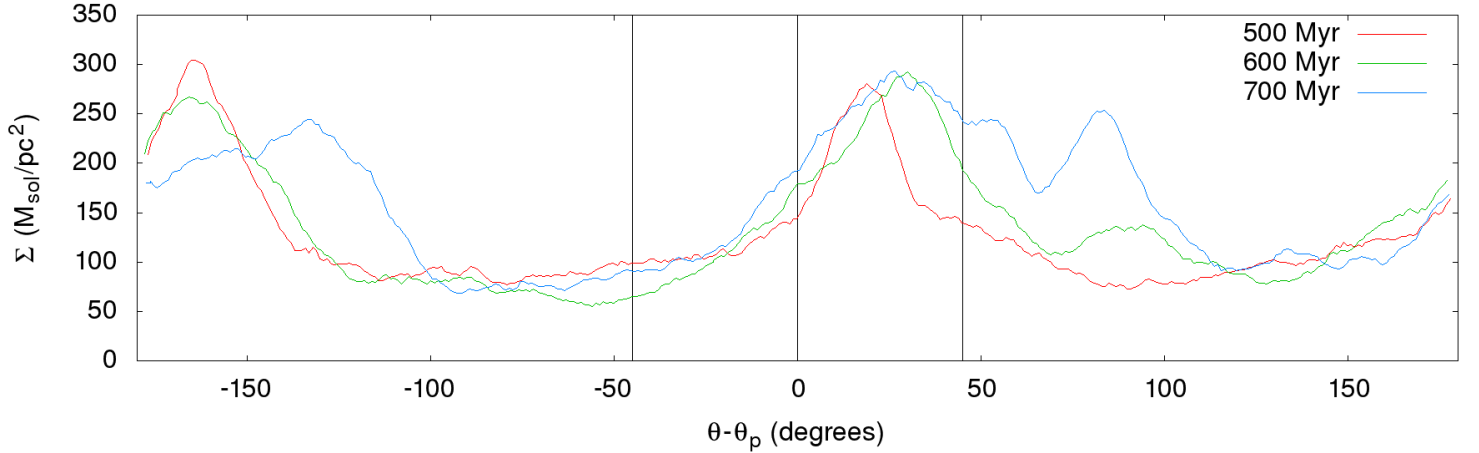


Figure 3. Surface density for our selected particle involved in outward migration (one of the asterisks in Figure 2a), at three separate times during migration. The x -axis shows the azimuthal angle, $\theta - \theta_p$, with respect to the angle of the particle. Surface density is calculated in an annulus at the particles radius with a width of $\pm 0.1 \text{ kpc}$ and is given in units of $M_{\odot} \text{ pc}^{-2}$. Rotation is in the positive θ direction so the particle lags the nearest density peak for the three times shown. Vertical lines at $\pm 45^{\circ}$ show region in which we measure the location of the nearest peak and its density. The angular difference $\Delta\theta$ between particle and nearest density peak is shown in Figure 4. The density of the nearest peak and radial migration rate for the same particle are plotted in Figure 5.

Figure 2a and 4a) existed less than a rotation period. Grand et al. (2012a) followed a single spiral density peak at a radius of about 5 kpc for 120 Myr at which time it disappeared. The spiral feature that they traced had a pattern speed (or angular rotation rate) that varied with radius and appeared to be corotating (see their Figure 5). They demonstrated that it induced radial migration in nearby stars. Grand et al. (2012a) commented, “if there are indeed several wave modes present, it is evident that they must conspire in a specific way in order to produce a spiral arm feature that is apparently corotating.” Grand et al. (2012a) also commented the lifetime of the spiral feature they followed was short. A similar short lived spiral feature was traced by Grand et al. (2012a) with a lifetime of 160 Myr near the end of a bar. The stars identified by Grand et al. (2012b) in a barred galaxy simulation with morphology similar to ours also migrated when they were near a short lived density feature.

2.3 Transient features caused by interference between patterns

Swing amplification spiral models (e.g., Fuchs 2001) require a few rotation periods for growth and fading of the spiral density wave. However, a density feature that is short lived can be produced when two spiral density waves interfere. When density peaks are coherent, a large density peak can be produced from the sum of the two amplitudes. This density peak should survive until the two spiral density waves are out of phase. Consider two spiral density waves with m_1 and m_2 arms each and patterns speeds, Ω_1 and Ω_2 , respectively. In the frame of the first pattern, the other pattern has speed $\Omega_2 - \Omega_1$. If initially both patterns have maximum at the same angle, after a time

$$t = \frac{\pi}{m_2} \frac{1}{|\Omega_2 - \Omega_1|}, \quad (1)$$

the second pattern would be 180° out of phase at the location of the first pattern peak. We can also consider how long it takes for the second pattern peak to reach the next minimum of the first pattern. The minimum of these two timescales gives a symmetrical coherence timescale

$$t_{coh} \sim \frac{\pi}{\max(m_1, m_2)} \frac{1}{|\Omega_2 - \Omega_1|}. \quad (2)$$

Interference peaks are long lived, (long t_{coh}), only if the pattern speeds of the interfering waves are similar. For patterns with more than one arm, the lifetime of an interference peak is shorter than a rotation period at radius r_0 as long as

$$\left| \frac{\Omega_2 - \Omega_1}{\Omega_0} \right| 2 \max(m_1, m_2) \gtrsim 1, \quad (3)$$

where Ω_0 is the angular rotation rate of a particle in a circular orbit at r_0 . We can see if this condition can be satisfied in the vicinity of the end of the bar end in our simulation. We take pattern speeds measured previously in our simulation (listed in Table 1 by Quillen et al. 2011). Using a bar angular rotation rate $\Omega_b \approx 40 \text{ km s}^{-1} \text{ kpc}^{-1}$ and a two armed inner pattern with $\Omega_s \approx 30$ (in the same units) and $\Omega_0 \sim \Omega_b(r_0/r_b)$ where r_b is the bar’s corotation radius, we estimate

$$4 \left| \frac{\Omega_b - \Omega_s}{\Omega_0} \right| \sim \frac{r_0}{r_b} \quad (4)$$

using $m = 2$ for both patterns. Thus condition equation (3) is satisfied outside bar’s corotation radius ($r_0 > r_b$) for the bar and the inner two-armed spiral pattern. The condition for a coherence time shorter than a rotation period would also be satisfied by a slower three-armed spiral pattern interfering with the bar.

The bar in our simulation has a length of 4 –5 kpc (corresponding to 0.6 –0.7 in log). However in the simulation the bar appears to be longer at time 550 Myr than at 700 Myr. If the feature that caused migration in our simulation is a result of interference between a bar and a spiral density wave, then we expect both spiral and bar are in phase during the migration. The addition of spiral waves near the end of the bar might also account for the some of the variations in morphology near the end of the bar, explaining why the bar appears to vary in length and how its ends curve at different times. At time 500 Myr, the bar extends to 0.8 (in log). Between 525 and 650 Myr, in the region between 0.6 and 0.9, one end of the bar progressively curves and becomes more tightly wound. Previous studies have also seen spiral features that appear to become increasingly tightly wound (e.g., Grand et al. 2012b). In other words the winding angle of a density peak appears to tilt as a function of time. Another way to describe this behavior is with a measure for the angular rotation rate of the density peak that depends on radius. A spiral feature that becomes more tightly wound also has a density maximum with angular rotation rate that varies with radius. Below, we will discuss interpretation of spiral features that wind up (increase in winding angle in time) or have angular rotation rate that is dependent on radius in terms of interference between steady patterns.

2.4 Describing the simulation density peaks in terms of interfering waves

We can test the possibility that transient structures in our simulation are due to spiral density wave interference by seeing if we can mimic the appearance of the density perturbations, seen in the simulation, with a simple interference model. In the same projection as shown in Figure 2a, we have summed three density perturbations each with a fixed pattern speed. Each perturbation is described as a surface density perturbation with a Gaussian amplitude

$$\Sigma(r, \theta, t) = \Sigma_i \exp\left(-\frac{(\log_{10} r - l_i)^2}{2w_i^2}\right) f(\phi_i(r, \theta, t)) \quad (5)$$

with function

$$f(\phi) = \cos(\phi) + 0.25 \cos(2\phi). \quad (6)$$

For each pattern the parameter Σ_i describes the density amplitude. The function, $f(\phi)$, is somewhat more peaked at $\phi = 0$ than a cosine and allows sharp features to be present in the surface density. The amplitude peaks at a radius r_i such that $\log_{10} r_i = l_i$, consequently l_i is a parameter that describes the mean of the radial region in log space that contains the wave. The amplitude extends a radial range controlled by the parameter w_i . We define a spiral argument for the i -th spiral density wave

$$\phi_i(r, \theta, t) \equiv \alpha_i \ln(r/r_b) - m_i(\theta - \Omega_i(t - t_0) - \theta_i). \quad (7)$$

The number of arms or azimuthally symmetry (for a bar) is set by m_i . The pattern speed is set by Ω_i and α_i controls the

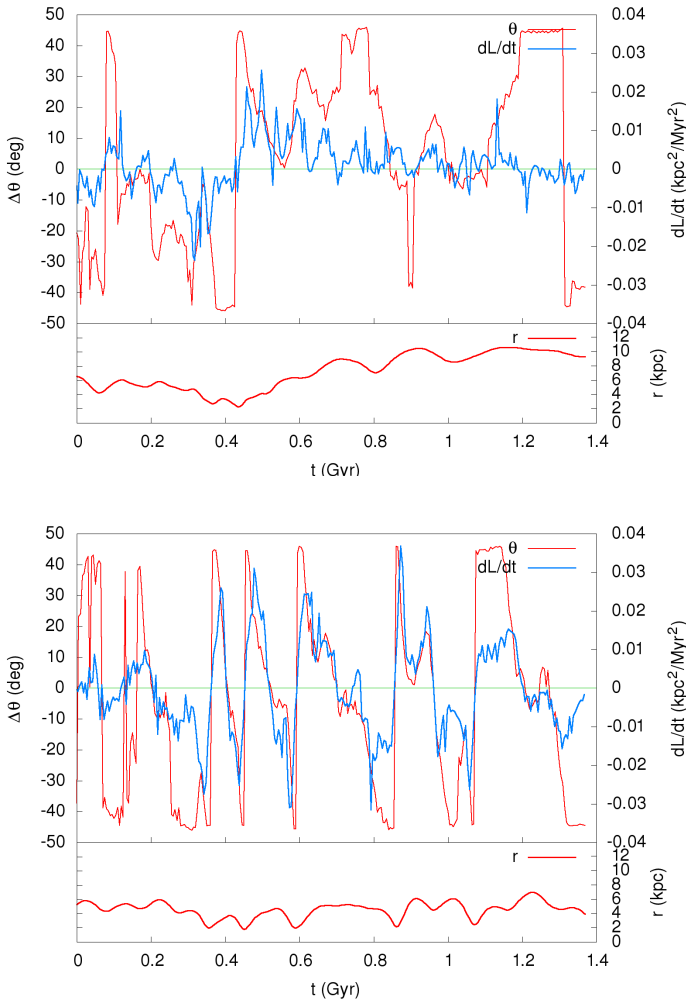


Figure 4. a) For a particle that migrates we plot the rate of change of angular momentum (\dot{L}) as a function of time as a blue line with axis on the right hand side. Also plotted, as a red line, is the angle to nearest density peak ($\Delta\theta$) with axis on the left hand side. Note that outwards migration (positive \dot{L}) only occurs when the particle lags the density (positive $\Delta\theta$). We also show particle radius as a function of time in the lower panel. Outwards migration primarily occurs when radial oscillations are not large. Units for \dot{L} are $\text{kpc}^2 \text{Myr}^{-2}$. b) Similar to a) except for a particle that does not migrate a significant amount during the simulation.

winding angle. The bar perturbation has $\alpha_i = 0$ but when $\alpha \neq 0$, the spiral perturbations are logarithmic. A logarithmic spiral density wave with m_i arms can approximately be described as having surface density and potential dependent on the angle ϕ_i and with amplitude slowly varying with radius. The offset of each pattern at time $t = t_0$ is set by a radius, r_b , and angle θ_i . Here the winding angle, γ_i , depends on $r d\theta/dr$ in a density peak with

$$\cot \gamma_i = \beta_i = \frac{\alpha_i}{m_i}. \quad (8)$$

A model that contains two spiral patterns and a bar is shown in Figure 2b with parameters listed in Table 1. The listed parameters are for each pattern: a pattern speed (Ω_i), number of arms (m_i), width parameter (w_i), winding parameter (α_i), log radius of maximum (l_i) and angular offset

(θ_i). Figure 2b, showing the model, can be compared to Figure 2a, showing the simulation. We have assumed rotation with $d\theta/dt = 0$, and trailing spiral patterns corresponding to negative α_i . The pattern speeds listed in Table 1 are given in terms of the bar's pattern speed and the offset angles given in terms of the bar's orientation at $t_0 = 550$ Myr, corresponding to the top left panels in Figures 2a and b. The pattern speeds, Ω_i , are given in units of the bar's angular rotation rate that is $2.3^\circ \text{Myr}^{-1}$ (equivalent to the $0.040 \text{ radians Myr}^{-1}$ or $40 \text{ km s}^{-1} \text{ kpc}^{-1}$ measured from a spectrogram and listed in Table 1 by Quillen et al. 2011); (to convert from radians Myr^{-1} to $\text{km s}^{-1} \text{ kpc}^{-1}$ multiply by 1000). At early times, (top panels in Figure 2b) the spiral features reasonably well match the simulation with morphology shown in Figure 2a. However, at later times, the model and simulation are increasingly different. The model is likely too simplistic. To better match the simulation we would probably require a model containing additional patterns, and with patterns that are not fixed in time but slowly vary as the bar slows down.

The two-armed structure in the model has an angular rotation rate of 34.4 and the three armed one has $28 \text{ km s}^{-1} \text{ kpc}^{-1}$. These patterns were not listed in Table 1 by Quillen et al. 2011 as prominent patterns in the simulation. However they do correspond to fast features seen in the spectrograms. The three armed structure corresponds to a peak at about 5 kpc at an angular frequency of $0.090 \text{ radians Myr}^{-1}$ shown in the spectrogram of Figure 6 by Quillen et al. (2011) (angular frequency is m times the pattern speed). The two armed one corresponds to a fainter feature just past the end of the bar at an angular frequency of 0.07 Myr^{-1} present in the spectrogram shown in see Figure 4 by Quillen et al. (2011), and that may be associated with a clearer feature in the $m = 4$ spectrogram (their Figure 5) at an angular frequency of about 0.14 Myr^{-1} .

The reasonable correspondence between the model Figure 2b and the simulation in Figure 2a the two figures suggests that an interference model can reproduce transient spiral features in this simulation. The feature causing migration of the star shown in Figures 2a (and crudely modeled in Figure 2b) likely appears and disappears due to interference between the fast two and three-armed structures with patterns listed in Table 1 and are consistent with faint peaks seen in the spectrograms.

Using the the bar and two-armed spiral pattern speed (and $m = 2$ for both) listed in Table 1 and equation (2) the coherence timescale for peaks arising due to positive interference is approximately 1.8 bar rotation periods where a bar rotation period is approximately 160 Myr. Similarly the coherence time between bar and three-armed and two and three armed structures is 0.6 and 1 bar rotation periods. These short coherence timescales are consistent both with the timescale we estimated for the lifetime of the peak causing stellar migration and discussed previously in section 2.2.

Table 1. Density Wave Model

Pattern	Ω_i	m_i	α_i	l_i	w_i	θ_i
Bar	1.00	2	0	0.33	0.23	0°
Two-armed	0.86	2	-3	0.71	0.14	-10°
Three-armed	0.70	3	-6	0.90	0.17	10°

A three pattern density wave model with parameters chosen to match the simulation at around 500 Myr. Here angular rotation rates for each pattern, Ω_i are given in units of the bar's angular rotation rate. The number of arms or symmetry in the case of the bar is given by m . The winding angle is determined from α_i and m_i using equation (8). The density peak is at a radius such that $l_i = \log_{10} r$. Each pattern extends over a radial range set by w_i . Each pattern is described by Equations 5 - 7 and using $\log_{10} r_b = 0.6$ with r_b in kpc. The amplitude of each structure has $\Sigma_i = 0.7$ in units of the azimuthally averaged value. Here the offset angle, θ_i , is given in terms of that for the bar that has major axis at 130° at time $t_0 = 550$ Myr, corresponding to the second panel in Figure 2a. The resulting density is shown at different times in Figure 2b. Parameters were adjusted so that the density field is similar to that seen in the simulation and shown in Figure 2a.

3 PROPERTIES OF PEAKS ARISING FROM INTERFERENCE BETWEEN TWO SPIRAL DENSITY WAVES

The corotation model for migration is consistent with the low eccentricities of migrating particles and that migration primarily takes place when a particle lags a density peak. However our spectrograms don't show patterns (other than the bar) that are strong in their corotation region. Furthermore the peaks that we see in our simulation causing migration survive less than rotation period and so are likely caused by interference between spiral density waves. Spiral patterns need not be long lived, however it is unlikely that spiral patterns appear and decay on timescales less than a rotation period. We consider the possibility that local peaks, caused by positive interference between two patterns, can cause stars to migrate. We first consider properties of local density peaks produced by interference. We then modify the corotation resonance model for migration in this setting.

3.1 Angular rotation rate of an interference peak

Using a model for two density waves we now compute the angular rotation rate of a local density peak caused by positive interference between the two waves. Spiral density waves are often described in terms of the number of arms, an amplitude (that is a function of radius), a winding angle and a pattern speed. Except for the number of arms, each of these parameters could vary in time, and their radial dependence could also vary with time. This is a large and poorly constrained multidimensional parameter space for variations. To separate between variations caused by single spiral patterns that vary in time, and phenomena caused by interference we can consider two fixed patterns that have different pattern speeds. We use a spiral argument for the i -th spiral density wave (similar to equation 7)

$$\phi_i(r, \theta, t) \equiv \alpha_i \ln r - m_i(\theta - \Omega_i t - \theta_i) \quad (9)$$

where we have dropped the constant r_b and the angle θ_i describes an angular offset at time $t = 0$. With two logarithmic spiral perturbations the mass surface density as a function of time

$$\Sigma(r, \theta, t) = A_1(r) \cos(\phi_1) + A_2(r) \cos(\phi_2) \quad (10)$$

The amplitude functions $A_i(r)$ we assume are slowly varying with radius.

Consider a location and time where there is a local density peak so that Σ has an extremum with $\frac{\partial \Sigma}{\partial \theta}(r_0, \theta_0, t_0) = 0$. By taking the derivative of equation (10) the extremum occurs where

$$A_1(r_0)m_1 \sin(\phi_1(r_0, \theta_0, t_0) + A_2(r_0)m_2 \sin(\phi_2(r_0, \theta_0, t_0)) = 0.$$

We consider small perturbations in time and angle about this moment and position; $t = t_0 + dt$ and $\theta = \theta_0 + d\theta$ and require that this new position and time is also a local density peak and so is also an extremum so that $\frac{\partial \Sigma}{\partial \theta}(r_0, \theta_0 + d\theta, t_0 + dt) = 0$. By expanding this partial derivative to first order in dt and $d\theta$ we can estimate $d\theta/dt$. To first order the density peak moves with angular rotation rate

$$\begin{aligned} \Omega_p = \frac{d\theta}{dt} &\approx \frac{m_1 A_1 \cos \phi_1 \Omega_1 + m_2 A_2 \cos \phi_2 \Omega_2}{m_1 A_1 \cos \phi_1 + m_2 A_2 \cos \phi_2} \\ &\sim \frac{m_1 A_1 \Omega_1 + m_2 A_2 \Omega_2}{m_1 A_1 + m_2 A_2} \end{aligned} \quad (11)$$

where in the second step we have assumed that the local density peak is near the density maximum of both waves where $\phi_1 \sim \phi_2 \sim 0$.

The above expression describes the angular rotation rate of the density peak. We see that its angular rotation rate lies between the the pattern speeds of the two density waves, with value depending upon the amplitudes of each wave. Consider a situation with the first wave faster than the second one, $\Omega_1 > \Omega_2$, and with peak amplitude at a smaller radius than the second one. In this case A_1 and A_2 are smoothly varying with radius and A_1 is high at small radii and A_2 high at larger radii. At an inner radius where the first wave dominates, equation (11) implies that Ω_p is near Ω_1 but at a radius where the second pattern dominates Ω_p would be near Ω_2 . The peak would effectively vary in pattern speed with pattern speed decreasing as a function of increasing radius. Density peaks with an angular rotation rate that depend on radius have been identified in simulations, for example see Figure 5 by Grand et al. (2012a) and Figure 8 by Grand et al. (2012b). The maximum angular rotation rate is that of the faster pattern, and this is consistent with the angular rotation rate of the feature identified by Grand et al. (2012b) approaching that of the bar at small radius (see their Figure 8). The variation in Ω_p with radius causes the winding angle of the density feature to vary in time or wind up (as shown in figure 7 by Grand et al. 2012b). We note that other types of transient models might also predict such behavior, for example swing amplification models predict that the winding angle varies in time as the amplitude varies. A swing amplified model would also effectively give a peak with angular rotation rate that varies with radius.

The above expression for the angular rotation rate (equation 11) does not depend upon α_i or the winding angles of the patterns. Consequently it can be used for $\alpha_i = 0$ and so can describe a bar-like perturbation that has a fixed

angle as a function of radius. We can consider interference between a fast bar perturbation and a slow local spiral perturbation. Outside a bar's corotation radius, the bar pattern speed would be faster than the local angular rotation rate. Spiral patterns are often observed in simulations to be strong inside their corotation radius (or at radii where the pattern speed is larger than the local angular rotation rate; e.g., Quillen et al. 2011). In a setting where a local spiral pattern interferes with perturbations from a bar, we would expect that the effective angular rotation rate $d\theta/dt$ of an interference peak between would lie between the bar's and the spiral's pattern and ranging at small radius with an angular rotation near that of the bar to near that of the spiral at larger radius. In this setting the effective angular rotation rate of the interference peak would necessarily pass a point where $d\theta/dt$ is equal to the local angular rotation rate and so the interference peak would act as if it were going through its corotation resonance. This is likely the situation in our simulation and causing migration. Bar corotation regions are seen as location where migration is common even after the formation of the bar (in our Figure 1, but also see Figure 7 by Minchev et al. 2012). However slow spiral structure in the vicinity of a bar would cause interference peaks with nearly corotating angular rotation rates. This may in part account for the efficacy of bar corotation regions in causing stellar migration.

3.2 Radial position of the maximum density

Above we considered the azimuthal location of peaks. We now consider the radial location of the maximum density in a local peak and how it would vary in time. In our simulation we see local peaks usually appear at a small radius and move outwards, but sometimes appear at a large radius and move inwards. We can try to understand the speed and direction of motion using the same model as we used above. A localized burst of star formation could be caused from density wave interference. As long as the amplitudes are only slowly varying in time and radius then the local density primarily depends on the arguments. When the two patterns lie directly on top of one another then the density is a maximum. Consider a radius, angle and time where the two waves constructively add or $\phi_1(r_0, \theta_0, t_0) = \phi_2(r_0, \theta_0, t_0) = 0$. Consider a nearby radius $r_0 + dr$ where the two waves also constructively add but at time $t_0 + dt$ so that $\phi_1(r_0 + dr, \theta_0 + d\theta, t_0 + dt) = \phi_2(r_0 + dr, \theta_0 + d\theta, t_0 + dt) = 0$. We can solve for $\theta_0 + d\theta$ using equation (9) for both angles,

$$\begin{aligned} \theta_0 + d\theta &= \frac{\alpha_1}{m_1} \ln(r_0 + dr) + \Omega_1(t_0 + dt) \\ &= \frac{\alpha_2}{m_2} \ln(r_0 + dr) + \Omega_2(t_0 + dt). \end{aligned} \quad (12)$$

Expanding to first order and relating dr to dt , we find that the density maximum moves inwards or outwards in radius at a speed

$$\left. \frac{dr}{dt} \right|_{peak} = \frac{r_0(\Omega_2 - \Omega_1)}{\alpha_1/m_1 - \alpha_2/m_2} = \frac{r_0(\Omega_2 - \Omega_1)}{\beta_1 - \beta_2}, \quad (13)$$

where we have defined a parameter

$$\beta_i \equiv \frac{\alpha_i}{m_i} = \cot \gamma_i. \quad (14)$$

Here larger β_1, β_2 correspond to more tightly wound structures.

We can see from equation (13) that the peak maximum moves slowly if the two pattern speeds are similar, and this is expected as they would remain in phase for longer. If we adopt $\Omega_1 > \Omega_2$ then the direction of motion depends on the sign of the denominator and this depends on the winding angles of each pattern (equation 8). If the faster pattern is more tightly wound than the other ($\beta_1 > \beta_2$), then the density maximum would move inwards, otherwise it would move outwards. In the first case we would expect a burst of star formation that progressively moves inwards in radius, and in the second case moving outwards in radius. Star bursts propagating inwards would occur if the center of the galaxy had more open spiral structure than the outer regions of the galaxy.

The denominator of equation (13) is only zero when the two waves have the same winding angle and so the two patterns are in phase at all radii simultaneously. If two patterns have nearly the same winding angles then the denominator is large. This implies that the peak is nearly in phase at all radii simultaneously. We would expect a burst of star formation across the density peak that is nearly coeval at all radii. We note that the above expression neglected variation of the amplitudes A_1, A_2 with radius and time, but expect these would not strongly affect the drift rate, \dot{r} , as long as the density variations are more strongly dependent on angle than radius.

It may be useful to put equation (13) in units of pc/Myr

$$\dot{r}_{peak} = 200 \text{ pc Myr}^{-1} \frac{(\Omega_2 - \Omega_1)}{\Omega_0(\beta_1 - \beta_2)} \left(\frac{v_c}{200 \text{ km s}^{-1}} \right). \quad (15)$$

There may be a progression of ages of star clusters and moving groups with stars closer to the Galactic center being younger in the Sco Cen region (Eric Mamajek, private communication). Such transient peaks would be expected within an interference model if the outer galaxy is more tightly wound than the inner galaxy.

4 MIGRATION BY LOCAL DENSITY PEAKS

Above we have illustrated how interfering spiral density patterns can cause a local density enhancement to appear for a short period of time. We now consider whether such a peak can induce stars to migrate. We first review a Hamiltonian model for migration caused by a corotation resonance based on the seminal work by Sellwood & Binney (2002).

4.1 Corotation resonance model for migration

For an axisymmetric system we can describe orbits in terms of a Hamiltonian that is a function of the angular momentum, L , and the momentum associated with epicyclic motion, J . These two momenta are conjugate to the an angle θ that is approximately the azimuthal angle in the plane, and the epicyclic angle, φ ;

$$H_0(L, J; \theta, \varphi) = g_0(L, J) \sim g_0(L) + g_1(L)J + g_2(L) \frac{J^2}{2}. \quad (16)$$

As the system is axisymmetric, the Hamiltonian does not depend on the two angles, so H_0, J and L are all constants

of motion. Above and on the right we have expanded the unperturbed Hamiltonian to second order in J . The angular rotation rate of a particle in a circular orbit in the unperturbed potential, $\Omega(L)$, is

$$\Omega(L) = \frac{\partial g_0(L)}{\partial L}. \quad (17)$$

The epicyclic frequency $\kappa(L) = g_1(L)$. For a flat rotation curve $g_0(L) = v_c^2 \ln L$, $\Omega(L) = \frac{v_c^2}{L}$ and $\kappa(L) = \sqrt{2}\Omega(L)$.

We can consider a logarithmic perturbation to the gravitational potential in the form

$$V(r, \theta, t) = \epsilon f(\beta \ln r - (\theta - \Omega_s t)) \quad (18)$$

where r is the radius, the perturbation has amplitude $\epsilon(t)$, pattern speed Ω_s , and winding angle γ , with $\cot \gamma = \beta$. We consider a system with θ increasing in the direction of rotation. In this case a trailing logarithmic spiral has $\beta < 0$. The above perturbation depends on radius rather than our action angle variables. If we take the low eccentricity limit and average over the dependence of r on the epicyclic angle then $r \sim L/v_c$ where v_c is the circular velocity with angular momentum L . In the vicinity of a corotation resonance (and distant from any Lindblad resonances and in the low eccentricity limit) the Hamiltonian depends on angular momentum L and azimuthal angle θ alone;

$$H(L, \theta) = g_0(L) + \epsilon(t)f(\beta \ln L - (\theta - \Omega_s t)). \quad (19)$$

where we have replaced r with L and removed an arbitrary constants from θ and t . Sellwood & Binney (2002) have illustrated that in the vicinity of a corotation resonance, the epicyclic amplitude is not affected.

It is useful to define an angle

$$\phi \equiv \beta \ln L - (\theta - \Omega_s t). \quad (20)$$

with time derivative

$$\dot{\phi} = \beta \frac{\dot{L}}{L} - (\dot{\theta} - \Omega_s). \quad (21)$$

The potential perturbation function, $f(\phi)$, may be periodic. For example the function $f(\phi) = \cos(m\phi)$ gives an m armed spiral structure. This type of perturbation is equivalent to the model discussed by Sellwood & Binney (2002) and shown in their Figure 6. Previously we discussed density perturbations using a similar form for the perturbations. Here we focus on perturbations to the gravitational potential.

Hamilton's equations (using the Hamiltonian of equation 19) are

$$\dot{L} = -\frac{\partial H}{\partial \theta} = \epsilon f'(\phi) \quad (22)$$

$$\dot{\theta} = \frac{\partial H}{\partial L} = \Omega(L) + \epsilon f'(\phi) \frac{\beta}{L}. \quad (23)$$

Inserting $\dot{\theta}$ and \dot{L} into the expression for $\dot{\phi}$ gives

$$\dot{\phi} = \Omega_s - \Omega(L). \quad (24)$$

The above equation implies that when $\Omega(L) \sim \Omega_s$ (in the vicinity of corotation), the argument ϕ is nearly constant and the angular momentum increases or decreases depending upon the sign on the right hand side of equation (22). As $\epsilon f(\phi)$ is the perturbation to the gravitational potential we can also write equation (22) (one of Hamilton's equations) in the following way

$$\dot{L} = -\frac{\partial \Phi}{\partial \theta} = -(\mathbf{r} \times \nabla \Phi) \cdot \hat{\mathbf{z}} \quad (25)$$

where Φ is the entire gravitational potential. The angular momentum drift, \dot{L} , arises from the torque from the non-axisymmetric portion of the potential perturbation. Lagging the potential minimum we expect $\epsilon f'(\phi) > 0$ corresponding to $\dot{L} > 0$. Particles lagging a potential minimum would migrate outwards.

A maximum migration rate is

$$\dot{L}_{max} \sim \max |\epsilon f'(\phi)| \quad (26)$$

leading to a maximum radial migration rate of order

$$\dot{r}_{max} \sim \frac{\dot{L}_{max}}{v_c}. \quad (27)$$

Note that the maximum torque on a particle can be directly estimated from the maximum tangential force at a given radius.

In the rotating frame with $\theta' = \theta - \Omega_s t$, the Hamiltonian becomes

$$K(L, \theta') = g_0(L) - L\Omega_s + \epsilon(t)f(\beta \ln L - \theta'). \quad (28)$$

As K is independent of time, it is conserved and known as the Jacobi integral. Expanding this Hamiltonian about the angular momentum corresponding to corotation or $L = L_s + J$, with $\Omega(L_s) = \Omega_s$,

$$K(J, \theta') = \text{const} - \Omega'(L_s) \frac{J^2}{2} + \epsilon f(\beta \ln L_s - \theta') + \dots \quad (29)$$

with $\Omega'(L) = -v_c^2/L^2$ for a flat rotation curve. This gives an equivalent description of the migration model in the corotating frame. Up to this point we have not assumed any particular form for the potential perturbation, only a pattern speed. Nevertheless the maximum migration rate can be estimated from the maximum strength of the derivative of the potential perturbation (equations 26, 27).

4.2 Corotation resonant width and eccentricity limit

In the WKB approximation a logarithmic spiral density perturbation comprised of a single Fourier component

$$\Sigma(r, \theta, t) = -S_m \Sigma_0 \cos(\alpha \ln r - m(\theta - \Omega_s t)) \quad (30)$$

has gravitational potential

$$V(r, \theta, t) \approx \frac{2\pi G S_m \Sigma_0}{|\alpha| r} \cos(\alpha \ln r - m(\theta - \Omega_s t)), \quad (31)$$

(computed with wavevector $k \approx \alpha/r$ as by Binney & Tremaine 1987). Here $S_m \Sigma_0$ is the strength of the m -th Fourier coefficient of the surface density. Σ_0 is the azimuthally averaged density and S_m is an amplitude in units of Σ_0 . Previously we have used a winding parameter $\beta = \alpha/m$ so that the argument can be written $\alpha \ln r - m(\theta - \Omega_s t) = m[\beta \ln r - (\theta - \Omega_s t)] = m\phi$. In this case the function f of Hamiltonian equation (19) is a cosine, and the perturbation strength for the potential (equation 18)

$$\epsilon = \frac{2\pi G S_m \Sigma_0 r}{|\alpha|}. \quad (32)$$

The Hamiltonian (equation 29) is similar to that of a pendulum. Shifting the angle θ' by a constant we can rewrite the Hamiltonian as

$$K(J, \theta') = \frac{v_c^2}{L_s^2} \frac{J^2}{2} - \epsilon \cos(m\theta') \quad (33)$$

where we have neglected the constant term in the Hamiltonian, assumed a flat rotation curve and flipped the sign from equation (29). The resonance width can be estimated by computing the energy of the separatrix ($K = \epsilon$ at $J = 0$, $m\theta' = \pi$) and then solving for J at $\theta' = 0$. The width of the resonance (peak to peak in J) is

$$\Delta J \approx 4\sqrt{\frac{|\epsilon|}{v_c^2}} L_s. \quad (34)$$

Here ΔJ describes the width of the corotation resonance and determines the maximum radial distance that a particle can migrate in the resonance;

$$\Delta r \sim \frac{\Delta J}{v_c} \sim 4\sqrt{\frac{|\epsilon|}{v_c^2}} r_s \quad (35)$$

where $r_s = L_s/v_c$. Using equations (32) and (35),

$$\Delta r \sim 0.9\text{kpc} \left(\frac{S_m}{0.15}\right)^{\frac{1}{2}} \left(\frac{r_s}{8\text{kpc}}\right)^{\frac{3}{2}} \left(\frac{\Sigma_0}{50M_\odot\text{pc}^2}\right)^{\frac{1}{2}} \left(\frac{\alpha}{17}\right)^{-\frac{1}{2}} \left(\frac{v_c}{200\text{km s}^{-1}}\right)^{-1}. \quad (36)$$

Here we have used a surface density similar to that of the Milky Way disk at the Sun's galactocentric radius (Holmberg & Flynn 2004), a parameter $\alpha = 17$ for $m = 4$ and a winding angle of 13° as preferred by some models for the Milky Way (Vallée 2008), and the 15% density contrast estimated by Drimmel & Spergel (2001). This suggests that unless the Galaxy experienced strong and open spiral arms, migration over large distances is unlikely.

Using the cosine perturbation we can also estimate the maximum migration rate using equations (26,27) and the derivative with respect to θ' of equation (31),

$$\begin{aligned} \dot{r}_{max} &\sim \frac{2\pi G S_m \Sigma_0 r_s}{\beta} \\ &\sim 2\text{km s}^{-1} \left(\frac{S_m}{0.15}\right) \left(\frac{r_s}{8\text{kpc}}\right) \left(\frac{\Sigma_0}{50M_\odot\text{pc}^2}\right) \\ &\quad \left(\frac{\beta}{4}\right)^{-1} \left(\frac{v_c}{200\text{km s}^{-1}}\right)^{-1}, \end{aligned} \quad (37)$$

(here $\alpha = m\beta$). Only if there are strong and open spiral arms is migration rapid. We see migration at a rate of about 20 km s^{-1} (see Figure 5) exceeding the value above. Grand et al. (2012b) show a migration rate (using their Figure 10) of about 1kpc in 20 Myr equivalent to 50 km s^{-1} . The migration seen by Grand et al. (2012a,b) and us is both more extreme and quicker than estimated above using parameters estimated for local Galactic spiral structure. We will discuss this issue in more detail below.

For a particle to migrate the distance given in equation (35), it must be captured as the pattern grows near $\phi \sim -\pi/2$ and at low L and then released at $\phi \sim \pi/2$ at higher L , as described by Sellwood & Binney (2002). The dependence of the resonant angle on $\beta \ln L$ does not affect the resonance width estimate (one can follow the same procedure to estimate the width of the separatrix). However the shape and normalization of the function $f(\phi)$ does affect the resonance width.

How low an epicycle (eccentricity) is required for capture into a corotation resonance? The eccentricity must be low enough that the angle, ϕ , remains within $\pi/2$ of the potential gradient extremum, otherwise the torque on the particle would oscillate instead of remaining positive or negative, as exhibited by the migrating and non-migrating particles shown in Figure 4. We consider ϕ as a function of r rather than angular momentum or $\phi = \beta \ln r - \theta'$. An orbit with eccentricity e has an apocenter of $r \sim r_0(1+e)$. Inserting the apocenter radius into the expression to ϕ we find $\phi \approx \beta \ln r_0 + \beta e$, consequently epicyclic variations cause a change in ϕ of order βe . To keep ϕ from varying by more than $\pi/2$ as the particle moves radially in the epicycle we require that

$$e \lesssim \frac{\pi}{2\beta} = \frac{\pi m}{2\alpha}. \quad (38)$$

The corotation resonance is likely to be ineffective for particle eccentricities above this value. Tightly wound patterns can only cause migration in extremely low eccentricity stars.

Previous studies have found that corotation resonances are only effective at causing migration among low eccentricity particles (see Figure 12 by Minchev et al. 2012 and associated discussion). Using the $\alpha_i = 6$ parameter for the $m = 3$ pattern from Table 1 listing our model patterns, equation (38) gives a maximum eccentricity of 0.8 for particles to be captured into a corotation resonance. However in section 2.1, we estimated that only particles with eccentricity $e \lesssim 0.2$ migrated, hence equation (38) overestimates the maximum particle eccentricity. We will discuss this issue again when we consider the Gaussian bar potential perturbation model below.

4.3 Migration by a thin Gaussian bar

When the potential perturbation is well approximated with a single Fourier component (equation 31, 30), then the maximum migration rate occurs at an angle $\phi = \pi/2$. However the density as a function of angle is poorly approximated by single Fourier component (see Figure 3) and we find that migration is taking place when the particle is 30° (not 90°) of the density peak. Similarly the extreme migrators shown by Grand et al. (2012b) were within $10 - 20^\circ$ of a density peak (see their Figure 14). We could expand the gravitational potential perturbation function in terms of Fourier coefficients with $f(\phi) = \sum A_m \cos m\phi$. However the maximum tangential force (and the angle at which the maximum is located) is then a function of the Fourier coefficients as the derivative of each component reaches a maximum at a different angle.

To take into account the narrowness of the spiral features, we describe a local density peak as a bar-like linear feature with a surface density profile (rather than in terms of Fourier components)

$$\Sigma(y) = \Sigma_p e^{-y^2/(2\sigma^2)}, \quad (39)$$

where Σ_p is the peak density subtracted by the mean density, and the density bar has full-width-half-max of 2.35σ . This description has the advantage that it is a function of only three parameters, the peak density, Σ_p , (above a background level), a width, described with σ , and an orientation angle. We assume that the density feature does not strongly depend

on the direction perpendicular to y . We orient the density feature with the winding angle γ , with $\gamma = 0$ corresponding to the feature azimuthally oriented and $\gamma = 90^\circ$ with the feature oriented radially. Here y increases in the direction perpendicular to the feature. For a tightly wound structure $\beta^{-1} = \tan \gamma \sim \gamma$.

The Fourier transform of the above density profile is also Gaussian with $\Sigma(k) = \Sigma_p \sigma \exp(-k^2 \sigma^2 / 2)$. In the thin disk approximation, and using Poisson's equation, each Fourier coefficient of the gravitational potential $\propto e^{iky - |kz|}$. Using a pillbox about the plane we can show that for each Fourier coefficient the gravitational potential¹

$$\Phi(k) = -\frac{\sqrt{2\pi} G \Sigma_p \sigma}{|k|} \exp\left(\frac{-k^2 \sigma^2}{2} + ik y\right). \quad (40)$$

Taking the y derivative and integrating over k

$$\frac{\partial \Phi}{\partial y} = 2\sqrt{2\pi} G \Sigma_p \int_0^\infty e^{-k^2/2} \sin\left(\frac{ky}{\sigma}\right) dk \quad (41)$$

$$= 4\sqrt{\pi} G \Sigma_p \text{DawsonF}\left(\frac{x}{\sqrt{2}\sigma}\right), \quad (42)$$

where the Dawson-F integral is defined as

$$F(x) \equiv \exp(-x^2) \int_0^x \exp y^2 dy. \quad (43)$$

The Dawson integral peaks approximately at $F(1) \sim 0.5$, consequently the maximum drift rate should occur for a particle located at a distance $x \sim \sqrt{2}\sigma$ from the peak or approximately at the half-width-half max position.

We can now consider a rotating logarithmic Gaussian bar with surface density

$$\Sigma(r, \theta, t) = \Sigma_p \exp\left(-\frac{(\beta \ln r - (\theta - \Omega t))^2}{2s^2}\right) \quad (44)$$

with angular width s . We can relate $s = \sigma/r$. For a Gaussian bar tilted at an angle γ we can approximate locally

$$\frac{\partial \Phi}{\partial \theta} \sim \frac{\partial \Phi}{\partial y} \sin \gamma. \quad (45)$$

The angular derivative of the gravitational potential

$$\frac{\partial \Phi}{\partial \theta} \sim 4\sqrt{\pi} G \Sigma_p \sin \gamma \text{DawsonF}\left(\frac{\phi}{\sqrt{2}s}\right) \quad (46)$$

with γ the winding angle and ϕ defined as in equation (20).

Using the derivative $d\Phi/d\theta$, we can estimate the maximum torque τ_{max} and from this the maximum drift rate $\dot{r} \sim \tau_{max}/v_c$ or

$$\dot{r}_{max} \sim G \Sigma_p 2\sqrt{\pi} \Omega^{-1} \sin \gamma \quad (47)$$

or

$$\dot{r}_{max} \sim 12 \text{km s}^{-1} \left(\frac{\Sigma_p}{50 M_\odot \text{pc}^{-2}}\right) \left(\frac{\sin \gamma}{24^\circ}\right) \times \left(\frac{r_0}{8 \text{kpc}}\right) \left(\frac{v_c}{200 \text{km s}^{-1}}\right)^{-1}. \quad (48)$$

Here we have used the typical 24° winding angle estimated for the spiral features in the simulation (Quillen et al. 2011)

¹ The integral of $\Phi(k)dk$ does not converge, however the integral should be cut off at small k due to the finite thickness of the disk.

and a surface density similar to that of the Milky Way disk at the Sun's galactocentric radius (Holmberg & Flynn 2004). The above estimate suggests that high density peaks are most effective at causing migration. The migration rate is only fast enough to cause significant migration within an orbital period if the surface density is of order $50 M_\odot \text{pc}^{-2}$. As mentioned previously, this presents a potential problem for migration models for the Milky Way as peak spiral amplitudes have been estimated at levels much below this (e.g., Drimmel & Spergel 2001).

The maximum drift rate occurs for a particle approximately at the half-width-half-max location and so is sensitive to the peak width. The particle must remain within a half-width of this location, hence the upper limit on eccentricity for migration particles must be modified from that estimated using a cosine potential perturbation (equation 38). Using an apocenter radius $r = r_0(1 + e)$ and keeping ϕ within angular width s of the maximum migration rate position we estimate that for a particle to migrate

$$e \lesssim \frac{s}{\beta}. \quad (49)$$

For $\beta \sim 2$ in our model (taking values from Table 1) and width $s \sim 30^\circ \approx 0.5$ radians from Figure 3 we estimate $e \lesssim 0.25$ and this is approximately consistent with our previous estimate (based on Figure 2a) that the maximum migrator eccentricity $e_{max} \sim 0.2$.

Our estimate for the migration rate (equation 48) depends on the strength of the potential term and this is set by the peak surface density of the feature. Using the Gaussian bar model we compare estimated migration rates to those measured in the simulation. In Figure 5 we show both the migration rate and density of the nearest spiral peak for our selected particle (with trajectory also illustrated in Figure 2a, 3, and 4). As expected, the migration rate is tightly correlated with the peak density of the nearest spiral feature. During the period of migration from 500 Myr to 700 Myr, the density Σ_p of the nearest density peak has values in the range of $100\text{--}250 M_\odot \text{pc}^{-2}$. Using a mean value of $\Sigma_p \approx 180 M_\odot \text{pc}^{-2}$ and equation (48) we estimate a migration rate of 40km s^{-1} . This is somewhat higher than the mean migration of about $20\text{--}30 \text{km s}^{-1}$, but we should remember that equation (48) estimates a maximum value and so we expect the actual value to be somewhat lower.

We have found that the Gaussian bar model successfully estimates the migration rate, the limiting eccentricity value for migration and the angular position of a particle that is rapidly migrating. In these ways the Gaussian bar model is superior to a model that approximates the potential perturbation with a single Fourier component. However, even though the derivative of the potential perturbation is well defined for the Gaussian bar, the potential itself is not, making it impossible to modify equation (35) to estimate the extent that a particle can migrate. Up to this point we have not considered how growth and variations in winding angle effect the migration model. However if migration is rapid, then a local approximation for the Gaussian bar is sufficient to estimate the migration. To estimate the extent that a particle can migrate we would have to take into account the time dependent form of the potential perturbation and the particle's trajectory (in ϕ) with time.

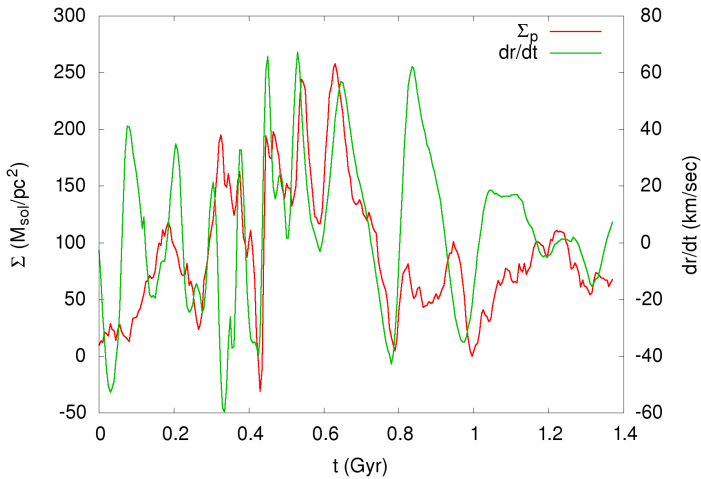


Figure 5. Peak density and migration rate. For the selected particle shown in Figure 4a the nearest peak mass surface density, Σ_p , subtracted by the mean density, is shown as a red line and has y -axis on the left. Also shown as a green line and with along with y -axis on the right, is the rate of radial migration, \dot{r} . Both Σ_p and \dot{r} are shown as a function of time. During the period of migration from 500 to 700 Myr, the peak density and migration rate are correlated, as we would expect from a corotation resonance mediated migration model. The rate of migration and peak density are approximately consistent with the maximum estimated using the Gaussian bar model (equation 48).

5 DISCUSSION AND SUMMARY

As have other studies (Grand et al. 2012a,b; Minchev et al. 2012), we find stars that migrate in radius in our N-body simulation. However spectrograms of the simulation do not show transient patterns that are strong near their corotation radius, presenting a difficulty for the corotation resonance model for migration (Sellwood & Binney 2002). We find that particles migrate outwards in the simulation when they are at low eccentricity and lag a short lived local density peak, confirming the results of previous studies (Grand et al. 2012a,b). Density peaks may not survive more than a rotation period, suggesting that they are not due to individual growing and decaying spiral density waves. We consider the possibility that they are due to interference between density waves that last with fixed amplitudes, pattern speeds or winding angles for dozens of rotation periods and so is not inconsistent with recent studies that suggest that spiral structure is transient (e.g., Sellwood 2011).

We have explored a simple model for interfering spiral density waves and find that they can produce short lived local density peaks and these, if they are sufficiently strong, can account for the migration seen in our simulation. The mechanism for migration due to a corotation resonance proposed by Sellwood & Binney (2002) can be modified to apply for a short-lived local density enhancement. Using a Gaussian bar model for the potential perturbation, estimates of the migration rate, angular offset between particle and spiral feature, and maximum eccentricity for migrators roughly agrees with the values measured in the simulation. We show that interference peaks can appear to rotate faster at smaller radii than outer radii (and so appear to wind up) as seen in

our and other simulations (Grand et al. 2012a). The angular rotation rate of an interference peak should lie between the pattern speeds of the two patterns that cause it. Nearly corotating interference peaks would be particularly likely to appear near the end of a bar due to interference between the fast bar and more slowly moving spiral patterns outside the bar. This may account for ongoing radial migration that is seen in simulations after bar formation and in the vicinity of the bar.

We can contrast a migration mechanism mediated by individual spiral density waves (as proposed by Sellwood & Binney 2002) and one mediated by short lived interference peaks. An interference peak can have a higher surface density than each individual pattern. As the distance migrated and speed of migration depends on the surface density, interference peaks can enhance migration. Many interference peaks can be produced over the lifetime of a few spiral density waves. This suggests that migration events could occur faster and more frequently than when considering a model where migration events only occur when a single pattern grows and decays. This may ameliorate the timescale problem as only a few dozen spiral density waves could arise and decay during the age of the Galactic disk, however a few times this number of interference peaks may arise during the same time if there are multiple spiral density waves present. With a single pattern, migration can only occur at the corotation resonance of the pattern. Interference peaks can have a variety of effective angular rotation rates, depending upon the amplitudes and patterns of the waves causing them. Consequently migration induced by interference peaks may be more pervasive than migration induced by individual spiral density waves.

The migration rate and the distance a star can migrate due to corotation resonance are dependent on the peak density in a spiral wave. As the stellar surface density decreases with increasing radius, migration due to corotation resonances may be less effective in the outer parts of the Galaxy. Furthermore as migration likely occurred near the Sun’s radius it is likely that spiral structure is either stronger than previously estimated (e.g., by Drimmel & Spergel 2001), or was stronger in the past than currently observed in the Galaxy. Better measurements of the spiral structure in the Galaxy are needed to make quantitative estimates of the extent of on-going radial migration.

Interference between spiral density waves can mimic transient-like behavior, including inducing migration as discussed here. Short lived density peaks can also cause localized bursts of star formation that can move across a galaxy. This picture of star formation differs from that expected with a single strong density wave that would produce a constant amplitude wave of star formation. We estimate that the rate that a burst of star formation moves across a galaxy depends on the winding angle of the two patterns. A burst would move inwards if the outer galaxy contains more tightly wound spiral structure than the inner galaxy. Future studies could probe for evidence of localized bursts of star formation in context with spiral structure models to better constrain the nature of spiral structure in galaxies. Future studies can also aim to quantify the statistics of migrating stars using interference mediated corotation migration models.

Acknowledgements. This work was in part supported by NSF through award AST-0907841. We thank NVIDIA for gifts of graphics cards. We thank Jerry Sellwood for helpful comments.

REFERENCES

- Adams, F. C. 2010, *ARA&A*, 48, 47
- Baba, J., Asaki, Y., Makino, J., Miyoshi, M., Saitoh, T. R., & Wada, K. 2009, *ApJ*, 706, 471
- Binney, J., & Tremaine, S. 1987, *Galactic Dynamics*, Princeton University Press, Princeton, NJ
- Bland-Hawthorn, J., Krumholz, M. R., & Freeman, K. 2010, *ApJ*, 713, 166
- Brown, A. G. A., Portegies Zwart, S. F., & Bean, J. 2010, *MNRAS*, 407, 458
- Bubar, E. J., & King, J. R. 2010, *AJ*, 140, 293
- De Silva, G. M., Freeman, K. C., Asplund, M., Bland-Hawthorn, J., Bessell, M. S., & Collet, R. 2007, *AJ*, 133, 1161
- Drimmel, R., & Spergel, D. N. 2001, *ApJ*, 556, 181
- Eggen, O. J. 1992, *AJ*, 104, 1906
- Elmegreen, D. M., et al. 2011, *ApJ*, 737, 32
- Fuchs, B., & Wielen, R. 1987, in *NATO ASIC Proc. 207, The Galaxy*, ed. G. Gilmore & B. Carswell (Dordrecht: Reidel), 375
- Fuchs, B. 2001, *A&A*, 368, 107
- Fujii, M. S., Baba, J., Saitoh, T. R., Makino, J., Kokubo, E., Wada, K. 2011, *ApJ*, 730, 109
- Grand, R. J. J., Kawata, D. & Cropper, M. 2012, *MNRAS*, 421, 1529
- Grand, R. J. J., Kawata, D. & Cropper, M. 2012, *MNRAS*, in press, arXiv:1202.6387
- Henry, A. L., Quillen, A. C., Gutermuth, R. 2003, *AJ*, 126, 2831
- Holmberg, J., & Flynn, C. 2004, *MNRAS*, 352, 440
- Jenkins, A., & Binney, J. 1990, *MNRAS*, 245, 305
- Lynden Bell D., & Kalnajs A. J., 1972, *MNRAS*, 157, 1
- Meidt, S. E., Rand, R. J., & Merrifield, M. R. 2009, *ApJ*, 702, 277
- Minchev, I., Famaey, B., Combes, F., Di Matteo, P., Mouhcine, M., & Wozniak, H. 2011, *A&A*, 527, 147
- Minchev, I., & Quillen, A. C. 2006, *MNRAS*, 368, 623
- Minchev, I., Famaey, B., Quillen, A. C., Di Matteo, P., Combes, F., Vlahic, M., Erwin, P., & Bland-Hawthorn, J. 2012, *A&A*, in press
- Naoz, S., & Shaviv, N. J. 2007, *New Astronomy*, 12, 410
- Portegies Zwart, S. F. 2009, *ApJ*, 696, L13
- Portegies Zwart, S. F., McMillan, S. L. W., & Gieles, M. 2010, *ARA&A*, 48, 431
- Quillen, A. C. 2003, *Astronomical Journal*, 125, 785
- Quillen, A. C., & Minchev, I. 2005, *AJ*, 130, 576
- Quillen, A. C., Dougherty, J., Bagley, M. B., Minchev, I., & Comparetta, J. 2011, *MNRAS*, 417, 762
- Roskar, R., Debattista, V.P., Stinson, G.S., Quinn, T.R., Kaufmann, T., & Wadsley, J. 2008, *ApJ*, 675, L65
- Roskar, R., Debattista, V. P., Quinn, T. R., & Wadsley, J. 2012, *MNRAS* in press, arXiv1110.4413
- Schönrich, R., & Binney, J. 2009, *MNRAS*, 396, 203
- Sellwood, J. A. 2011, *MNRAS*, 410, 1637
- Sellwood, J. A., & Carlberg, R. G. 1984, *ApJ*, 282, 61
- Sellwood J. A., Binney J., 2002, *MNRAS*, 336, 785
- Toomre, A. 1990, *Dynamics and Interactions of Galaxies* (Berlin: Springer), 292
- Toomre, A., & Kalnajs, A. J. 1991, *Dynamics of Disc Galaxies* (Gothenburg: Goteborgs University), 341
- Vallée, J. P. 2008, *AJ*, 135, 1301
- Wada K., Baba J., & Saitoh T. R., 2011, *ApJ*, 735, 1
- Widrow, L. M., Pym, B., & Dubinski, J. 2008, *ApJ*, 679, 1239
- Wielen, R., Fuchs, B., & Dettbarn, C. 1996, *A&A*, 314, 438
- Wielen, R. 1977, *A&A*, 60, 263